Visible Light Imaging of Small Animals

A thesis submitted in partial fulfillment of the requirement for the degree of Bachelor of Science in Physics from the College of William and Mary in Virginia.

By

Kevin Smith

Dr. Robert E. Welsh, Advisor

Williamsburg, VA

May 2003

Abstract:

A visible light imaging system constructed from commercially available products is described. The utility of this detector system in the context of Bioluminescent and Fluorescent imaging is assessed through studies of the effects of temperature on CCD performance, expression of green fluorescent protein in Xenapous frog embryos, attenuation of light by biological tissue, and the overall performance of this imaging system.

Acknowledgements:

I would like to thank my advisor, Dr. Welsh, for the support and encouragement that led to the completion of this project. It has been a privilege to have him as my advisor for the past three years. I would also like to thank Dr. Eric Bradley and Dr. Margaret Saha of the department of biology for their advice and support. Finally I would like to thank the Howard Hughes Medical Institute for interest in and generous support of undergraduate research projects like this one.

Table of Contents:

Table of Figures

Introduction:

Current research in medical biology is in part dependent on advances in medical imaging systems. In addition, current trends in biomedicine value the use of imaging methods that provide humane treatment of the animals involved (1). This poses problems to laboratories interested in the study of small animals, as access to *in vivo* imaging technologies is somewhat limited, and alternative techniques either rely on expensive radioisotopes or require that the specimens be studied *in vitro* (1, 2). The development of reliable, cost effective *in vivo* imaging systems is thus of considerable value to laboratories engaged in small animal research.

A successful imaging technique must provide temporal and spatial assays of the biological process of interest while not significantly altering the process itself. In many studies, the principle focus is a process at the molecular level. Thus an effective imaging strategy must be sensitive to minute changes in distribution and function of an assayed substance over time. This study will weigh the benefits and drawbacks of an imaging technology that exploits the properties of visible light, and will describe an attempt to construct a cost-effective optical imaging device of this type using commercially available equipment.

Background:

Introduction to Medical Imaging

All imaging modalities rely upon the interpretation of energy interacting with biological tissue (3). To convey the benefits offered by visible light imaging (VLI), it is first necessary to discuss the theory behind this imaging modality. A formal discussion has been forgone below in the interest of brevity, however, more complete treatments of the topic can be found in (3-6).

In-vivo Imaging Modalities

X-ray computed tomography (X-ray CT), single photon emission tomography (SPECT), positron emission tomography (PET), ultrasound, and nuclear magnetic resonance imaging (MRI) are all well established *in vivo* imaging modalities that have far-reaching applications in biology (1). While each is an invaluable biomedical imaging tool, none provide a means of assaying gene expression, cell evolution, or transmission in animals (2).

Visible Light Imaging

VLI utilizes the properties of light emitted by an organism as a result of either external stimulation (fluorescence), or a byproduct of an internal biological process (bioluminescence). Both methods of light production provide suitable methods for evaluating models in molecular biology, specifically, gene expression and regulation.

Fluorescence

In vivo fluorescence imaging may involve either the introduction of fluorescent dyes to the sample tissue, or the labeling of a gene with a fluorescent tag by methods standard in molecular biology (1). This method of imaging is common in small laboratories as it is a relatively inexpensive means of modeling gene expression.

The use of fluorescent dyes has two inherent drawbacks: as cells divide and multiply, the ratio of dye to cell matter in the sample reduces, thus limiting the utility of this method in assays of cell population growth. Also, an external light source is required for fluorescence to take place, doubling the path length of incident light. Since the major limiting factor of VLI is the loss of light output due to scattering in animal tissue, this type of modality is of limited utility in assays of large tissue samples.

Bioluminescence

Bioluminescence imaging (BLI) exploits the properties of luciferase, a family of photo-proteins that can be isolated from a large variety of light-emitting organisms from diverse genetic backgrounds (7). Since these organisms are very distant relatives, there are many chemically unrelated forms of luciferase. Light with the emission spectra in the range of 400nm to 620nm is produced when the enzyme reacts exergonically with its substrate luciferin in the presence of molecular oxygen (7). Genes that produce luciferase can be cloned and transferred to other organisms using standard methods of molecular biology.

The advantage of this modality is the inherently low background noise: animal tissue without luciferin will not fluoresce. However, the utility of bioluminescence is still limited by the attenuation of light through biological tissue. The principle absorption of

light in mammalian tissues is caused by hemoglobin, which absorbs light with wavelengths of up to approximately 600nm (1). Since many forms of luciferase emit broad emission spectra, a large portion of which is of a wave length of over 600nm, bioluminescence has proven effective for *in vivo* applications.

Possible non-invasive applications of BLI range from assays of tumor growth (8) to studies in developmental biology (9) to characterizations of the spread of infectious viruses, such as HIV, in animals (10, 11). Unfortunately, commercially available BLI units are generally very expensive. The goal of the project described here is to construct a device that provides a small laboratory with the benefits offered by BLI techniques, without the high costs imposed by commercial systems.

Charge Coupled Device Cameras

Charged-coupled device (CCD) cameras have been favored for use in astronomy since the early 1980s since they are as much as ten times more sensitive than the fastest films (12) and provide a near-linear response (13). Digital cameras containing CCD devices are now widely used in commercial, professional and scientific contexts, including VLI.

CCD detectors

At the heart of any CCD camera is a two dimensional photosensitive array of silicon pixels that has a function analogous to the role of photographic film in traditional cameras. This surface is responsible for the acquisition of images, as shown in figure 1.

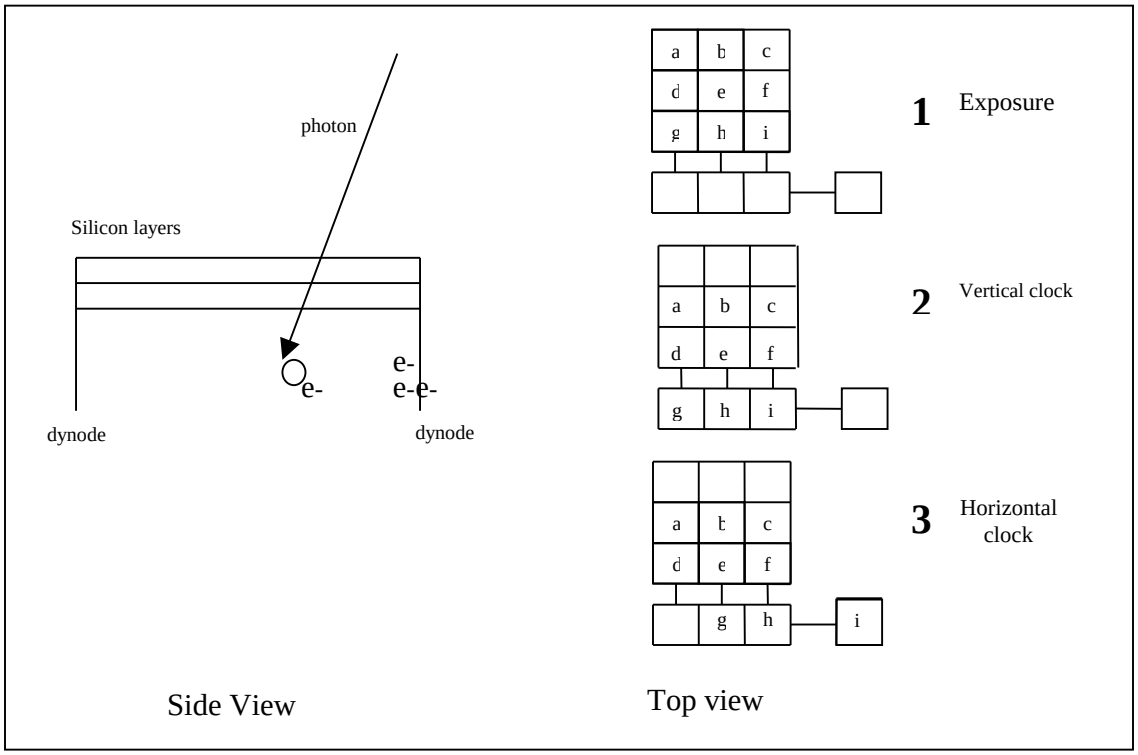

Figure 1: Side and Top Views of the process of exposure. Incident photons strike the surface of the detector and dislodge electrons which are collected on dynodes (left). These charge packets are fed to the preamp through a series of vertical and horizontal clock pulses (right). The alphabetical symbols a-i in the top view represent charge packets stored on the ccd chip. The number of electrons in a charge packet is proportional to the number of photons that struck the corresponding photo pixel during exposure.

Each pixel represents a rectangular region where incident photons are converted to electrons via the photoelectric effect and stored as packets of charge. During an exposure, an amount of charge proportional to the number of incident photons builds up in each pixel. After the exposure ends, a regulated sequence of clock pulses is responsible for transferring the accumulated charge packets to another array of pixels shielded from light (to prevent the buildup of additional charge). Another series of clock pulses then sends the signal in serial fashion through an analogue-to-digital (ADC) converter to a computer, which converts the charge packet into a numerical value. The

signal is then sent to a computer, where a composite image is assembled using a similar, but reverse algorithm.

Noise

The process described above is subject to several types of noise, each of which limits the ultimate signal to noise ratio (S/N) of images produced. Fortunately, much of this noise can be minimized through certain procedures.

Statistical noise

The number of photons produced by the image during exposure (N) is randomly distributed, and is thus analogous to the number of raindrops falling in a bucket over time (14). The statistical variance is equal to the square root of the number of photon events detected (n):

$$\text{var}(N) = \sqrt{n}$$

So at best, one can evaluate the number of incident photons as

$$N = n \pm \sqrt{n}$$

A longer integration time implies more photon events and a fractionally smaller statistical variance, thus one can minimize statistical noise by taking longer exposures.

Thermal noise (Dark Current)

In silicon, electrons can be spontaneously generated due to thermal statistic events. These electrons contribute to what is commonly referred to as dark current (figure 2), measured in the number of electrons per second (13). Thermal noise is thus measured as

$$T_n = \sqrt{D_c t}\ ,$$

where T_n represents thermal noise, D_C represents dark current, and t represents time.

A study of the effect of temperature on dark current is discussed below. In general, dark current is reduced by half for every 7°C the CCD detector is cooled, thus one benefits greatly from cooling the detector.

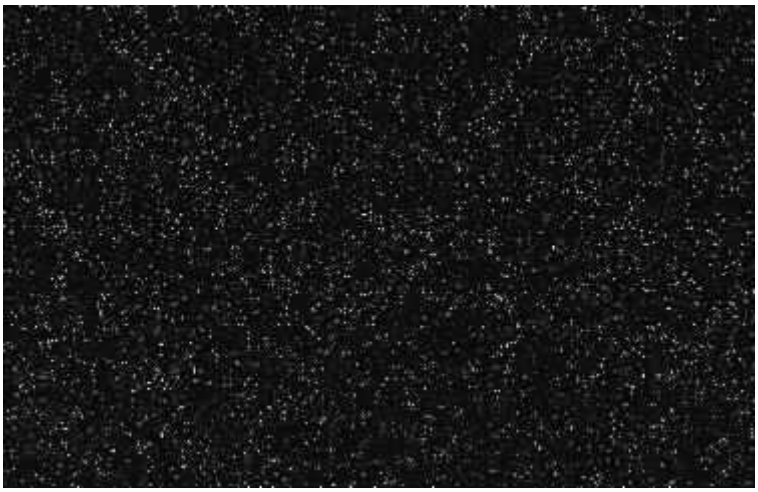

Figure 2: Image taken without a light source shows dark current (bright pixels) caused by statistical thermal noise in the CCD chip.

CCD detectors are typically cooled using liquid nitrogen, frozen carbon dioxide tablets, or Peltier-effect coolers. Liquid nitrogen provides the most effective cooling solution, as the detector reaches temperatures as low as -196°C. However, the cost and inconvenience of maintaining a constant supply of liquid nitrogen may make this method undesirable for small laboratories. Dry ice tablets (- 80°C) can be equally cumbersome (14), consequently many cameras are designed with Peltier cooling systems.

The Peltier cooling effect utilizes the properties of a thermocouple: current is passed through a junction of two dissimilar metals, causing one side of the junction to head up while the other side cools down. The cold side may be thermally isolated, creating a refrigerating system that can be used to cool the CCD chip. This method of cooling is less efficient than the other methods described above, however, the

temperature of the camera may be regulated to a high degree of accuracy (14). Regardless of the method used to cool the detector, it is always essential to hermetically seal the detector region to exclude moisture and keep the dew point below the CCD temperature.

Readout/Transfer noise

The process of transferring packets of charge to the memory bank and through the pre-amp stage results in the loss of electrons. This noise (s_e) can be quantified as

$$s_e = \sqrt{nNe} \ ,$$

where e is the loss in transfer efficiency, n is the number of transfers made, and N is the number of transported charges (13). Readout noise is therefore a product of the design of the CCD camera, usually specified by the manufacturer, and typically measured in electrons lost per transfer.

Sensitivity noise

Each pixel in the CCD detector is subject to imperfections and crystal impurities. Sensitivity noise refers to the variation in signal from one position on the detector to another. This noise also includes impurities in filters and or lenses, and can be corrected for by incorporating an image of a uniformly distributed light source during image calibration, as described below.

Electrical noise

The electronics of the CCD detector can be responsible for a finite amount of noise. Like readout noise, this noise is predominately a product of detector design. Additional contributions to electrical noise include interference with other electrical

devices. Thus the quality of transistors, the AD converter, and shielding from external electromagnetic radiation, such as radio waves, is particularly important in product design.

Experimental Setup:

Figure 3: A light tight box (background) contains the imaging apparatus. The ST-6 CCD camera (black) is supported by an adjustibe lab stand. A blue lab jack positioned beneath the camrea serves as a image bed, and can be vertially adjusted to alter the focal length.

Camera Specifications

Funding provided by the Howard Hughes Medical Institute enabled the purchase of a used ST-6 peltier cooled CCD camera made by Santa Barbara Instrument Group (SBIG), a company specializing in the manufacture of astronomical instruments.

The camera features a Texas Instruments TC-241 CCD chip with a pixel size of 27x11.5 micrometers. The camera adds consecutive horizontal pixels two by two to give an effective pixel area of 23x27 micrometers. The array has 91,000 pixels total, for a total photosensitive area of 8.6x6.5mm. The dark current at -30°C is 10 electrons per second, readout noise is 30 electrons, and the camera has a 16-bit ADC, thus a number

between 1 and 65536 (this number is proportional to the number of electrons in a particular charge packet) is returned to the computer for every photo-pixel.

The experimental apparatus and the flow of information are shown in figures 3 and 4. Amplified digital data is sent from a serial port on the back of the ST-6 camera to a central processing unit contained in a separate box that serves as the housing for the power supply. Another data cable connects the CPU with an IBM PC, which is used for data acquisition, storage, and processing.

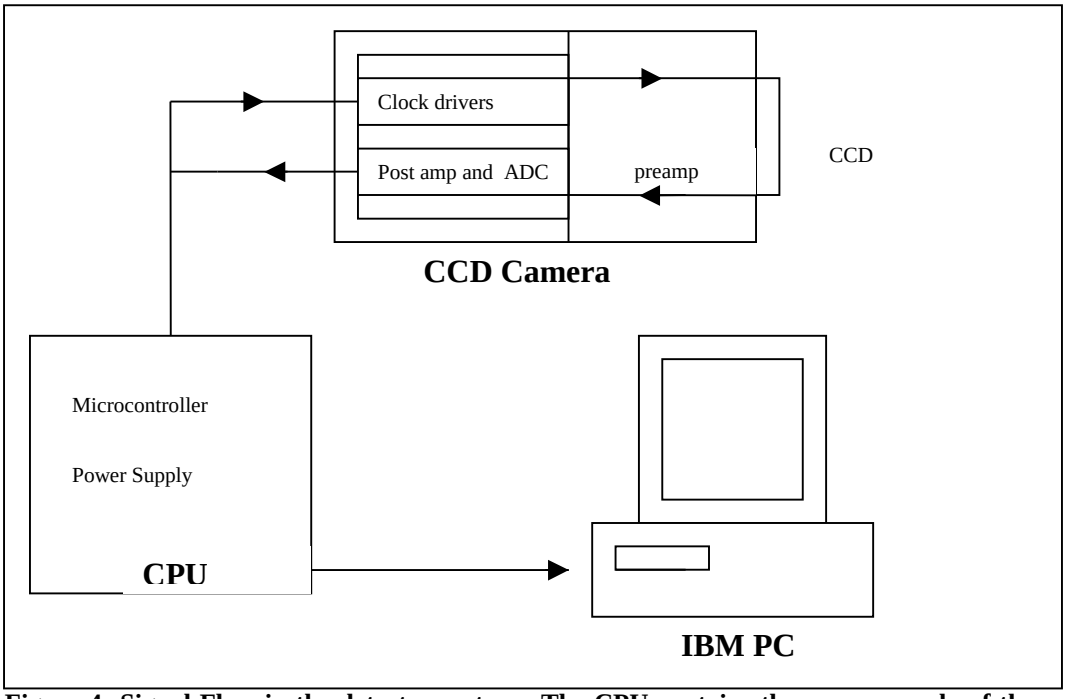

Figure 4: Signal Flow in the detector system. The CPU contains the power supply of the camera and hosts the microcontroller which is responsible for sending temperature control and shutter control signals to the CCD camera. The camera itself houses the clock drivers and the pre and post amplifiers. Output is sent from the camera through the CPU to an IBM personal computer.

Dark Box

The camera is optically sealed from the environment in a dark box constructed out of plywood (background of figure 3). Holes were cut in the side of the box to allow power cables to pass to the camera and the ultraviolet light source. A large door secured

with window latches allows access to the inside of the box. Care was taken to ensure that the box is completely light-tight. Even with integration times on the order of 10 minutes, light leakage remains sufficiently below background to avoid detection.

Ultraviolet Source

A high intensity ultraviolet source provides monochromatic light for fluorescence imaging. The light generates high–intensity ultraviolet light with a selectable wavelength of either 365nm or 254nm. This light source is not a radiation hazard, however, protective eye glasses must be worn when one operates the device.

Filters/Lenses

A standard "Computar" lens model number 1213 lens with an "f-number" of 1.3 and a lens diameter of 12.5mm serves as our main camera lens. A 508nm dichotic filter with a central wavelength tolerance of 2nm and full width half maximum (FWHM) tolerance of 2nm is attached to the camera face. A 405nm dichotic filter with the same tolerance specifications is mounted on the face of the ultraviolet source. Thus, the light to stimulate fluorescence has a central wavelength of 405nm, and we observe the fluorescent light with a central wavelength of 508nm, the central wavelength emitted by Green Fluorescent Protein.

Since the intent of this experiment is to image very low-intensity light from a small animal, the focal length is typically set to 1 foot, and the aperture is kept wide open.

Software

All image processing is done by a data acquisition program entitled CCDOPS provided by SBIG. The CDOS interface enables control of the camera's temperature,

shutter speed, and exposure time, and provides standard imaging processing algorithms (described below) which are commonly used in data analysis.

Image Processing

Reducing the level of noise through filtering drastically improves the integrity of images. Figure 4 represents raw data taken from a 5-minute exposure of 5 cotton balls under UV light, two of which were dyed with fluorescein. The CCD chip was held at a constant temperature. Note the level of noise is such that the signal is almost lost.

Since most of the noise is due to dark current, one can improve the signal to noise ratio by subtracting a dark frame from the initial image. A dark frame is simply an image taken with the same temperature and exposure time as the initial image, but without a light source. Since thermal noise is reproducible, subtracting the dark frame (figure 6) will result in improved signal and less noise (figure 7). The resulting image can then be enlarged and viewed in false color for maximum contrast (figure 8).

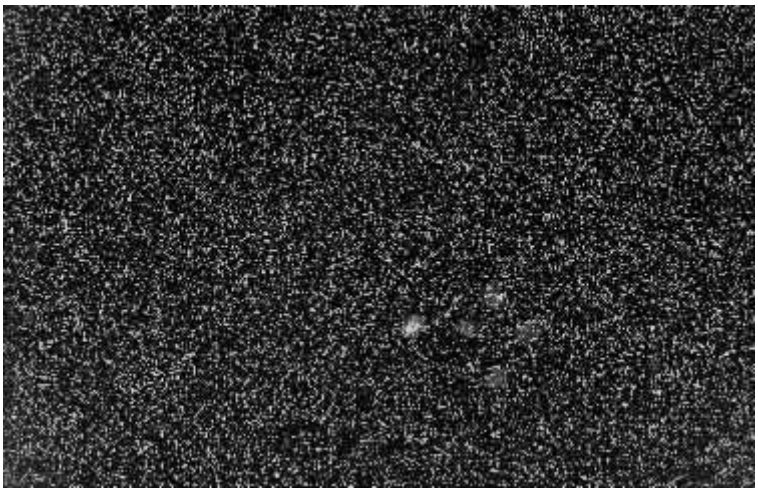

Figure 5: Unprocessed Raw Image of 5 cotton balls under UV light. Exposure time was one minute, and camera temperature was -30°C. Two balls were stained with Fluorescein. Only one stained ball is visible, the other four (three unstained and one stained) are virtually lost in the noise.

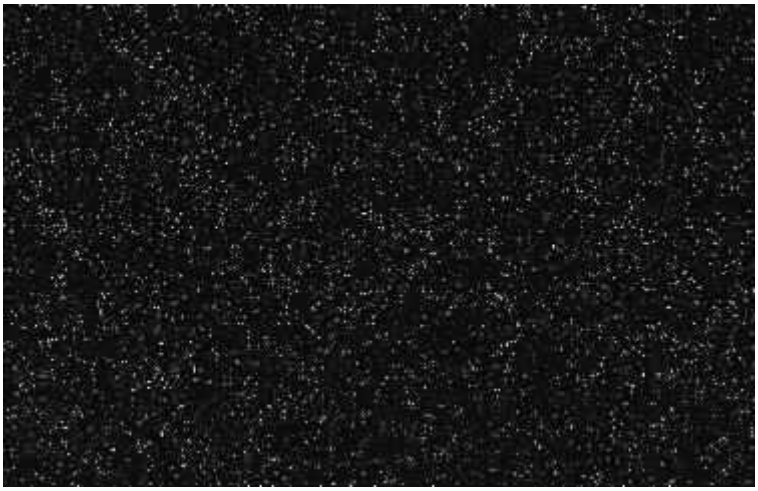

Figure 6: Dark Frame corresponding to Figure 5. This image was taken under the same conditions as figure 5, but with the shutter closed. Note the similarity in figures 5-7.

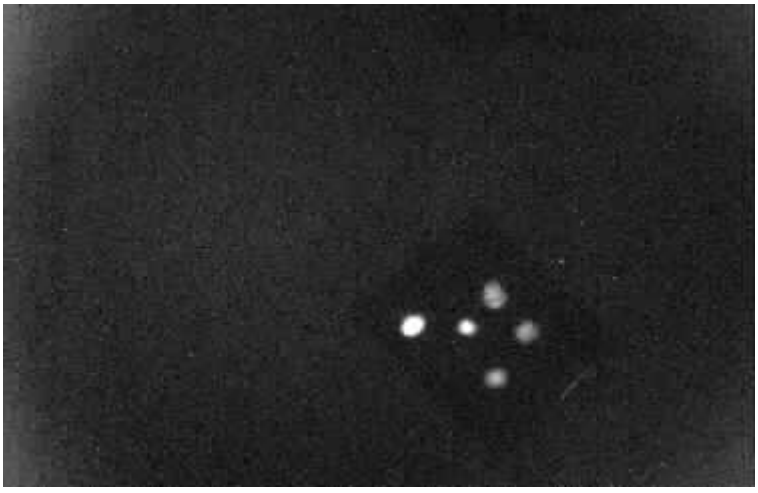

Figure 7: Composite image created by subtracting figure 6 from figure 5. Note the greatly improved signal: it is possible not only to see the individual cotton balls, but to discern which ones were dyed with fluorescein .

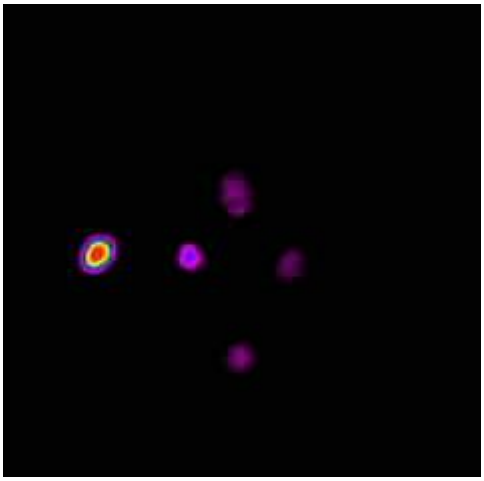

Figure 8: Final Processed image. False color was added. Red regions correspond to high levels of photon output. Purple regions correspond to levels just above background (black).

Once the dark image had been subtracted from the raw image, corrections were made for sensitivity noise. A flat-field image of a uniform white source was taken prior to the experiment. The dark-subtracted image was then divided by the flat field image to produce figure 8. The process as a whole can be modeled as:

$$final = \frac{raw - dark}{flatfield}$$

The flat field image appears in the denominator because sensitivity noise affects both the raw image and the dark image.

Each of the above operations is performed in CCDOPS. Additional operations that can be performed on data include contrast enhancement, sharpness and pixel interpolation (an algorithm that accounts for the slightly rectangular pixels on the CCD chip).

Experimental Results:

Noise as a Function of Temperature

As described above, the amount of noise in an image that is produced by dark current is heavily dependant upon temperature. To verify this, images were taken of four fibers under ultraviolet light with the CCD held at various temperatures ranging from room temperature to -30°C (figure 9). We are currently unable to operate at temperatures below this value, as we are unable to dissipate excess heat from the surface of the detector.

Data from this experiment can be found in table 1. Counts represent the value returned by the ADC averaged over a square of 5x5 pixels. Noise events were sampled from a region where there was no signal. Graph 1 is a plot of noise with respect to decreasing temperature.

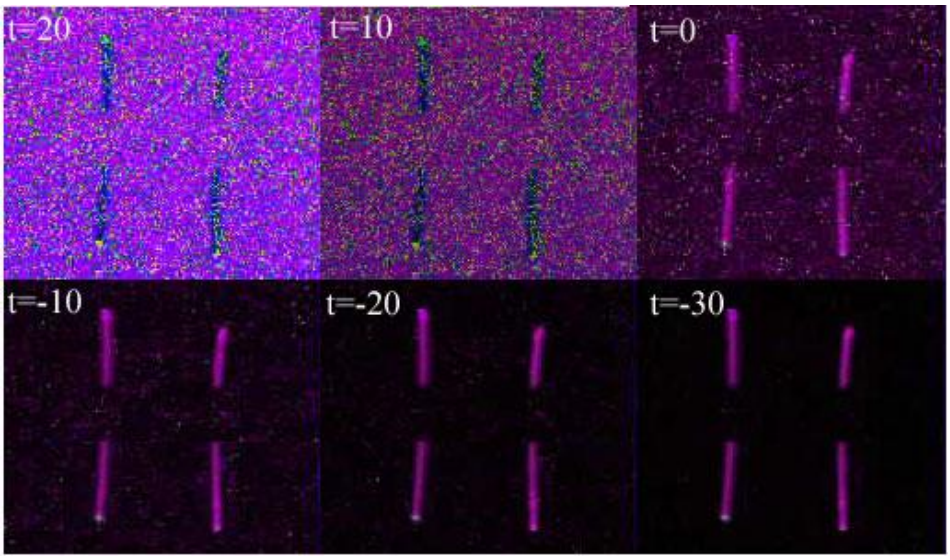

Figure 9: Noise as a function of temperature (t). Each image was given artificial color and cropped for display purposes. None of the images were corrected for dark current. Note the difference between the upper left and lower right images.

Table 1: Noise as a function of temperature

Temperature (°C)	20	10	0	-10	-20	-30
Noise (counts)	34428.21	4758	1385	612	343	276

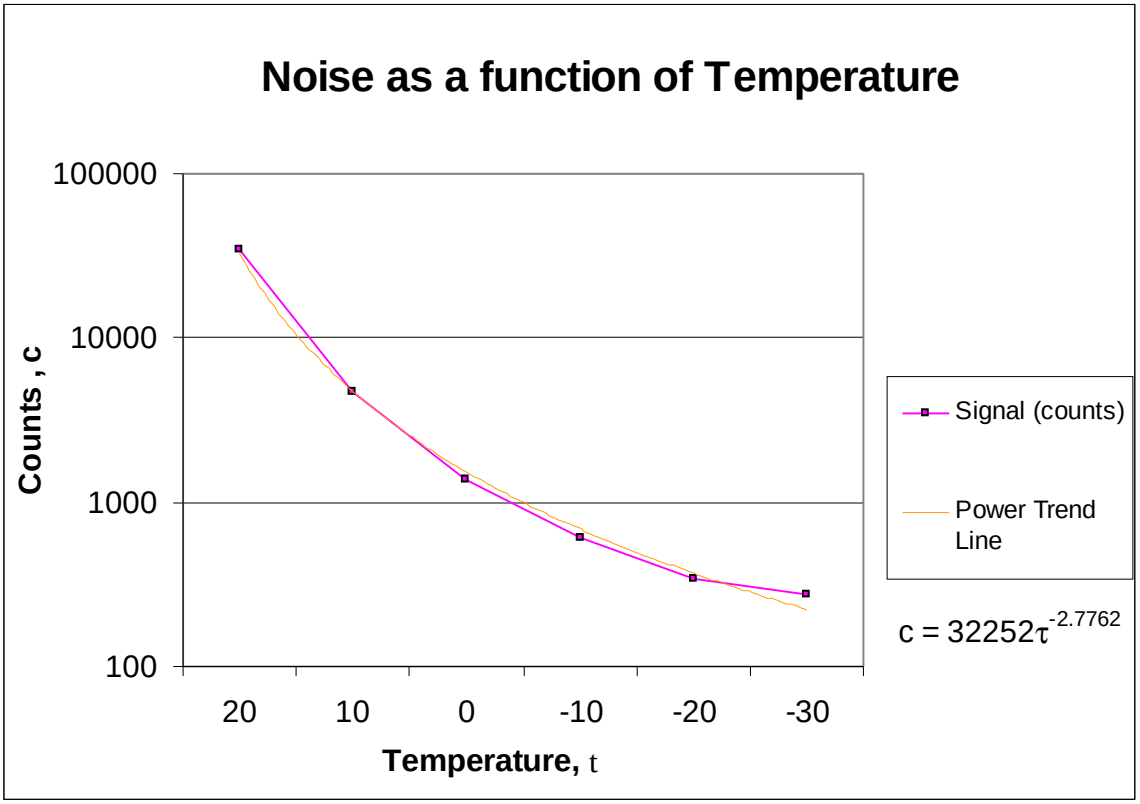

Graph 1: Noise as a function of temperature. The data from table 1 was plotted (purple points) and given a least squares fit (yellow line). The purple line represents linear extrapolation between data points.

A trend line (least squares fit) was fitted to the data to obtain an approximate formula of the relationship between noise and temperature. Based on the data collected, the noise in an image may be modeled as

$$counts = a\,t^{-b}$$

where α and β are parameters that depend on exposure time and source intensity.

Fluorescein

For effective fluorescence or bioluminescence imaging, one must be able to detect low-intensity light. Imaging small animals demands additional sensitivity at the expense of resolution, since one typically images all or part of an animal, as opposed to a cluster of cells. An attempt was made to assess the utility of such an imaging system through tests of the sensitivity and resolution of the camera.

Fluorescein is a compound typically used in gene expression studies. It absorbs blue light, with peak absorption and excitation wavelengths occurring between 465nm and 490nm. Fluorescence occurs at wavelengths of 520nm-530nm (yellow-green). Two cotton balls with diameters of about 8mm were each dyed with small but unequal amounts of fluorescein and placed on a piece of flat black tape among three other plain white cotton balls of roughly the same size. The tape was then placed under 405nm ultraviolet light and imaged through a 508nm dichotic filter for 300 seconds. Figure 10 represents the processed image. One can clearly discern a difference between dyed and clean cotton, thus proving that fluorescence imaging is a very real possibility with this detector system. Background levels were found to have on average 100 counts (appears black in the picture below); the purple regions in the image correspond to counts of about 1300, while the blue and green regions have average counts of 26000 and 39000, respectively.

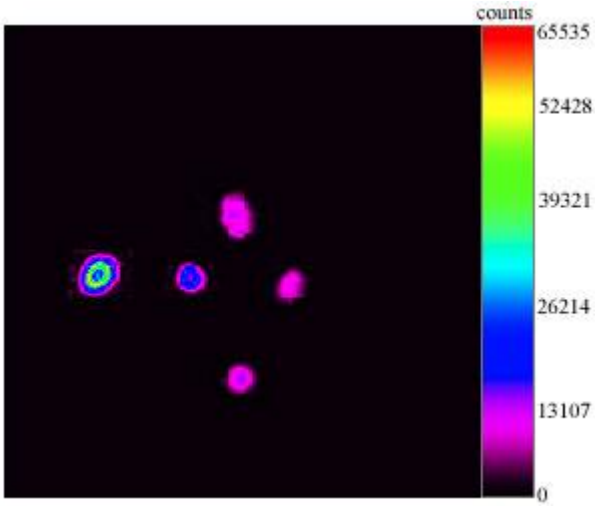

Figure 10: 5 cotton swabs. The two left most have been stained with an unequal amount of fluorescein. The balls that were not stained (purple) are roughly ten times background. The left most ball (green) was 15 times background.

Expression of GFP in Xenopus Frog Embryos

Efforts to observe autofluorescence or bioluminescence in living organisms were not as fruitful. Xenopus frog embryos were tagged with green fluorescent protein (GFP), a protein commonly used in molecular biology. GFP has an excitation wavelength of 400nm with a smaller excitation peak at 475nm, and has a fluorescence peak of 509nm. A sample of several hundred frog embryos (diameters of approximately 1mm) was placed under the same ultraviolet light with a peak of 405nm and imaged for 120 seconds with the CCD held at -20°C. No effort was made prior to the experiment to determine which frog embryos expressed the protein. There is little, if any, detectible difference between transgenic and normal frog embryos (see figure 11).

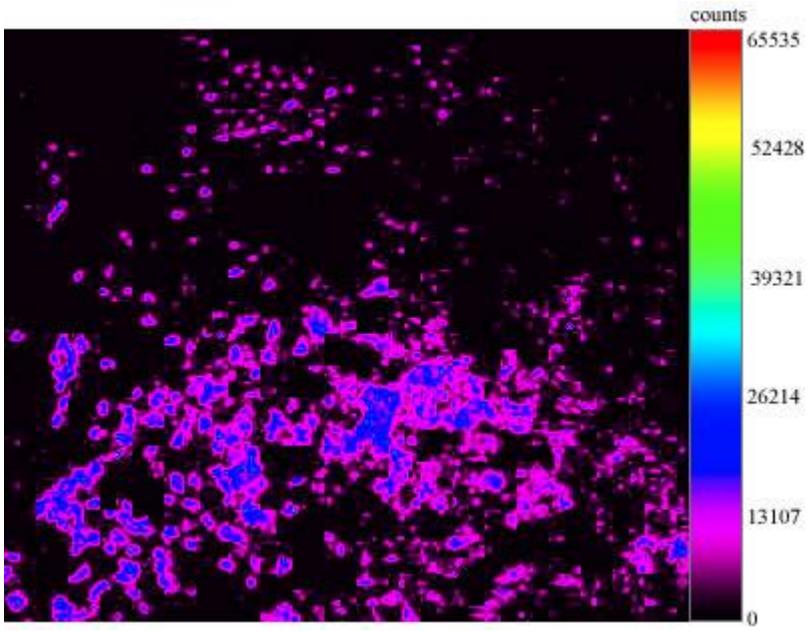

Figure 11: Green fluorescent protein expression in xenapous frog embryos. The embryos (purple, blue) appeared 10 to 20 times background (black). The width of the base is 20cm. Image time was 120 seconds.

After the above image was taken, efforts were made to isolate the embryos that expressed GFP. A subsequent image (figure 12) was taken three days later of embryos known to bioluminesce under the same time and temperature conditions. The embryos in this image, which has been enlarged to show detail, the embryos have grown 2-3mm. The results proved disappointing, as the sides of the container holding the sample reflected more light than the frogs were able to produce. However, we were able to resolve individual embryos, as the camera has a resolution of approximately 1mm.

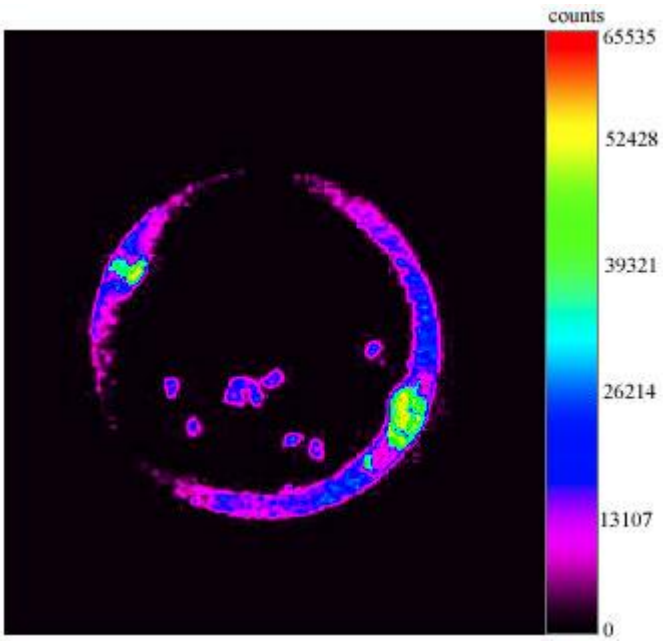

Figure 12: Green Fluorescent protein expression in xenapous frog embryos. This image was taken two days after figure 11 and enlarged to show detail,; one can easily see individual frog embryos (blue spots). The diameter of the container (large ring) is 10cm.

Attenuation of Light by Animal Tissue

Efforts were made to qualitatively assess the relationship between tissue depth and light absorption. A mouse was sacrificed, and two green fluorescent fibers were placed in the intestinal region, which we defined via a surgical skin window. One fiber was placed beneath the stomach, and another fiber was placed beneath the intestinal track. The goal of the experiment was to observe the level of light output once the whole specimen was placed under an ultraviolet lamp. The resulting image is reproduced below (figure 13).

We were able to observe fluorescence in the fibers; however, a large amount of scattering prevented us from resolving the spatial dimensions of the green fibers. Instead, the region of tissue directly above the fibers appeared as two unresolved spots. We

concluded that our detector system is able to detect fluorescence through as much as 0.25cm of tissue (roughly the depth of the stomach and intestinal region), however, we are currently unable to observe gene expression on the cellular level.

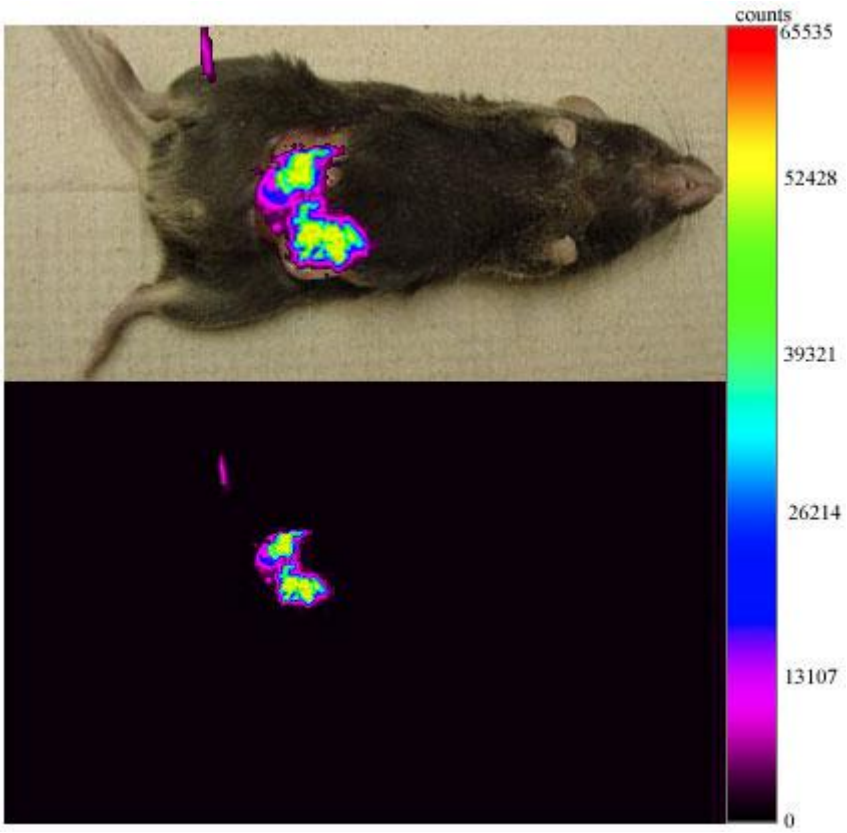

Figure 13: Attenuation of light in animal tissue. The bottom image was resized and superimposed on the mouse (top image) to show spatial orientation. The tube-shaped anomaly to the upper left of the mouse is part of the fiber that was not properly shielded.

Conclusion

A common concern with current biomedical imaging modalities such as X-ray scanning, single photon emission computed tomography, magnetic resonance imaging, and positron emission tomography, is that often one is unable to assess the microscopic and molecular behavior of key molecules in the assayed biological process (15). A visible light detector system is capable of in vivo imaging in real time, as it exploits the advantages offered by charged couple device cameras. The project described above represents an ongoing attempt to construct such an imaging device using commercially available equipment of moderate cost, thereby providing small laboratories with the benefits of this imaging modality without the restrictions cause by the expense associated with similar commercial systems.

To some extent, this goal has already been actualized, as we have shown that we are easily able to resolve objects of 1mm, and to observe fluorescence in an isolated sample. Lowering the temperature of the CCD chip through the incorporation of an additional cooling device will help us limit the effects of dark current, thus opening new possibilities for low intensity light imaging.

The detector system described above was built out of commercial materials with a total cost of under $2000. Existing systems typically cost a factor of 10 times as much. While these professional quality systems offer better resolution and sensitivity, it has been shown that it is possible to construct a device that would be useful to small laboratories engaged in small animal research.

References

1. Contag C., Bachman M., Advances in Vivo Bioluminescence Imaging of Gene Expression. *Annual Review of Biomedical Engineering,* January, 2002.

2. Oshiro M. Cooled CCD versus intensified cameras for low-light video applications and relative advantages. *Methods Cell Biology* 1998 56:45-62

3. Sprawls, Perrry. Physical principles of medical imaging. Madison, Wis: Medical Physics Pub. 1995

4. Kevles, Bettyann. Naked to the Bone: medical imaging in the twentieth century. New Brunsqick, NJ: Rutgers University Press, c1997.

5. Doby, T. Origins and development of medical imaging. Carbondale: Southern Illinois University Press, 1996.

6. Shung, Kirk. Principles of Medical Imaging. San Diego: Academic Press, 1992.

7. Ray P., Paulmurugan R., Berger F., Phelps M. E., Iyer M., and Gambhir S. S., Noninvasive Quantitative Imaging of Protein-Protein Interactions in Living Subjects. *Proceedings of the National Academy of Sciences,* vol. 99, no. 5., March 2002.

8. Sweeny T., Mailander V., Tucker A., Olomu A., Zhang Q., Cao Y., Negrin R., Contag, C. Visualizing the Kinetics of Tumor-cell Clearance in Living Animals. *Proceedings of the National Academy of Sciences.* Vol. 96, no. 21, October 1999.

9. Lipshutz G., Gruber C., Cao Y., Hardy J. Gaensler M. *In Utero* Delivery of Adeno-Associated Viral Vectors: Intraperitoneal Gene Transfer Produces Long-Term Expression. *Molecular Therapy* vol.3, no.3, March 2001.

10. Rocchetta H. Boylan C., Foley J., Iverson P., Letourneau D., McMillian C. Validation of a Noninvasive, Real-Time Imaging Technology Using Bioluminescent *Escherichia coli* in the Neutropenic Mouse *Thigh Model of Infection, Antimicrobial Agents and Chemotherapy*, Jan. 2001: 129-137

11. Francis K., Joh D., Bellinger-Kawahara C., Hawkinson, M., Purchio T. and Contag P. Monitoring Bioluminescent Staphylococcus aureus infections in living mice using a novel luxABCDE construct. *Infection and Immunity*, June 2000 p3594 – 3600.

12. Berry, Richard. The CCD camera cookbook: how to build your own CCD camera. Richmond, VA: Willmann-Bell, Inc. 1994.

13. Martinez, Patrick. A practical guide to CCD astronomy. Cambridge, New York: Cambridge University Press, 1998.

14. Berry, Richard. Choosing and Using a CCD camera: a practical guide to getting maximum performance from your CCD camera. Richmond, VA: Willmann-Bell, 1992.

15. Contag P., Contag C., Olomu N., Stevenson D. Bioluminescent Indicators in Living Mammals. *Nature Medicine,* vol.4, no.2, Feb. 2002.

16. Cho, Z. Foundations of medical imaging. New York : Wiley, c1993.

17. Bellingham, Wash. Handbook of Medical Imaging: SPIE press 2000. v.1,2,3

18. Imaging Detectors in high energy, astroparticle and medical physics: proceedings of the UCLA International Conference. Singapore; River Edge, NJ: World Scientific Publishing Co. 1996

19. International Conference on Information Processing in Medical Imaging: 15th International Conference, IPMI'97 Poultney, Vermont, USA, June 9-13, 1997.